J Mater Sci (2010) 45:64–73
DOI 10.1007/s10853-009-3891-z

Chlorinated polyethylene nanocomposites: thermal and mechanical behavior

Sritama Kar · Pradip K. Maji · Anil K. Bhowmick

Received: 4 April 2009 / Accepted: 14 September 2009 / Published online: 1 December 2009

Abstract Chlorinated polyethylene (CPE) nanocomposites prepared with natural and organically treated montmorillonite (MMT) clays by solution intercalation method were investigated. X-ray diffraction and transmission electron microscopy techniques showed separation of organically modified clay MMT layers and indicated formation of exfoliated nanocomposites. Fourier transform infrared spectroscopy results showed interaction between the CPE matrix and the clay intercalants of Cloisite® 30B and Cloisite® 15A (natural MMT modified with quaternary ammonium salts). Organically treated MMT clays were found to be better dispersed in CPE in comparison to natural MMT clay. Mechanical testing showed enhanced tensile strength, Young's modulus, and storage modulus of chlorinated-polymers/organically treated MMT clay nanocomposites. Significant improvements in the above properties were obtained with Cloisite® 15A nanoclay. The temperature, at which maximum degradation occurred, was higher for the nanocomposite having 5 wt% Cloisite 15A than that of neat CPE. Differential scanning calorimetric results revealed that the same composition also absorbed more heat during the heating, indicating better thermal stability. CPE rubber nanocomposite could be a promising heat resistant polymeric material.

S. Kar
School of Polymers and High Performance Materials,
The University of Southern Mississippi, 118 College Drive
#10076, Hattiesburg, MS 39406-0001, USA

P. K. Maji · A. K. Bhowmick (✉)
Rubber Technology Centre, Indian Institute of Technology,
Kharagpur 721302, India
e-mail: anilkb@rtc.iitkgp.ernet.in; director@iitp.ac.in

Present Address:
A. K. Bhowmick
Indian Institute of Technology, Patna 800013, India

Introduction

Nanocomposites have become a new promising area in the field of polymer research. The new class is composed of a polymer matrix and a filler of either natural or synthetic mineral particles. Since the invention of layered silicate/polyamide nanocomposites by Toyota Co. (Tokyo, Japan) [1, 2], polymer layered silicate nanocomposites (PLSN) have attracted great interest of researchers in the world both in industry and in academia. This is due to the fact that they often exhibit remarkable improvement in the characteristics of the material, such as better mechanical properties [3, 4], ionic conductivity [5, 6], or permeability [7]. Scientists around the world have subsequently investigated various polymer nanocomposites from thermoplastics. The nano-concept is highly relevant and very advantageous for rubber composites, and nano-reinforcement has been proven to be an extremely effective and necessary way for rubber applications [8–10].

Success of plastics nanocomposites greatly impels the study on PLSN based on rubber matrices. Co-coagulating rubber latex and layered silicate aqueous suspension is an easy method to prepare layered silicate/rubber nanocomposites wherein pristine clay is utilized instead of organic clay [11–13]. Some silicate/rubber nanocomposites such as fluoroelastomer [14, 15], polyurethane [16], acrylonitrile–butadiene rubber, ethylene–propylene–diene monomer [17, 18], natural rubber [19, 20], polybutadiene rubber, and styrene–butadiene rubber [21] with excellent properties and unique phase structure have been prepared by different methods. Ganguly et al. [22] successfully applied atomic

force microscopy for comprehensive nanoscale surface and bulk morphology characterization of thermoplastic elastomeric triblock copolymers: poly[styrene-*b*-(ethylene-*co*-butylene)-*b*-styrene] having different block lengths and their clay-based nanocomposites.

But chlorinated polyethylene (CPE)/montmorillonite (MMT) systems have been much less reported in the literature [23]. CPE is an important and widely used rubber. It is one of the most important high temperature resistant synthetic rubbers with excellent thermal stability, low-temperature toughness, and electrical insulating properties. It has been extensively used in electrical insulation, sealing, etc.

This study has focused on morphology and mechanical and thermal properties of CPE/layered silicate nanocomposites, and is intended to provide a basis for assessing them as additives in practical CPE formulations. Given that they are highly dependent on filler surface characteristics, orientation, and dispersion. The mechanical and thermal properties are also expected to provide a sensitive measure of the degree of exfoliation and hence complement other methods of characterization such as transmission electron microscopy (TEM) and wide angle X-ray scattering (WAXS). In general, the methods for the preparation of rubber–clay nanocomposites include in situ polymerization, solution, and melt intercalation, wherein organically modified silicate has been employed [24–26]. In this article, CPE/clay nanocomposites were prepared by solution blending of the rubber and clay, and their structures and properties were studied in detail. The main challenge that arises with these layered smectite clays concerns the possibility to obtain an exfoliated structure by solution blending, in order to improve the interfacial interactions governing the thermal and mechanical properties of the composite material.

Experimental

Materials

CPE used was Tyrin® 3652 (36% chlorine) obtained from a chlorination process of linear high-density polyethylene. Three commercial types of nanoclay based on MMT were used in this study: Cloisite® Na^+, Cloisite® 15A, and Cloisite® 30B from Southern Clay Products (Gonzales, TX, USA) (Table 1).

Compounding and vulcanization

5 wt% of clay dispersion was prepared by using methyl ethyl ketone via sonication for 20 min. Then the dispersion was added separately into the methyl ethyl ketone solution of CPE containing 5% of zinc oxide and 4% of magnesium oxide (rubber grade), and then drying it off at 25 °C for 2 days. Vulcanization was followed in an oscillating disc rheometer (Monsanto model 100S) at a temperature of 150 °C and oscillating arc of 3°. The rubber compounds were cured in a hydraulic press at 150 °C for the optimum cure time calculated from the cure curves. All the formulations of the CPE composites are tabulated in Table 2.

X-ray analysis

X-ray diffraction (XRD) was carried at room temperature by using Philips Diffractometer PW 1830 generator equipped with a Cu K_α ($\lambda = 0.154$ nm) source. The diffractograms were collected in 2θ ranges from 1.8 to 10, where the basal reflection of the interlayer d spacing appeared at a scanning rate of 2°/min. The composites were analyzed as pressed films and the clay as powder.

Table 1 Description of nanoclays used

Sample and short designation	Organic modifier	Modifier concentration (meq/100 g of clay)	Gallery distance (nm)
Cloisite®Na^+ (Na)	None	–	1.2
Cloisite® 30B (30B)	Methyl, tallow (~65% C18; ~30% C16; ~5% C14), *bis*-2 hydroxyethyl, quaternary ammonium	90	1.9
Cloisite® 15A (15A)	Dimethyl, dehydrogenated tallow (~65% C18; ~30% C16; ~5% C14), quaternary ammonium	125	3.4

Table 2 Compound designations of CPE nanocomposites

Compound designation	CPE-A	CPE-B			CPE-C	CPE-D
		CPE-B1	CPE-B2	CPE-B3		
Composition	CPE(100)/ ZnO (5%)/ MgO (4%)	CPE(100)/ZnO (5%)/MgO (4%)/ Na^+MMT (5%)	CPE(100)/ZnO (5%)/MgO (4%)/ Na^+MMT (10%)	CPE(100)/ZnO (5%)/MgO (4%)/ Na^+MMT (20%)	CPE(100)/ZnO (5%)/ MgO (4%)/ Cloisite® 30B (5%)	CPE(100)/ZnO (5%)/ MgO (4%)/ Cloisite® 15A (5%)

Transmission electron microscopy

Dispersion of clays in the rubber matrix was studied by TEM (JEOL 2010). The CPE composite films were cut using ultra-cryo-microtoming technique and were placed on copper grid. The films were then analyzed under an accelerating voltage of 200 kV.

Fourier transform infrared spectroscopy analysis

To investigate the interaction between the clay and the polymers, the polymer was dissolved in methyl ethyl ketone and the pre-dispersed clay was added to the polymer solution. The solution was mixed vigorously with mechanical stirrer for 3 h at 60 °C. Fourier transform infrared spectroscopy (FTIR) studies were carried out in dispersive mode on thin film samples (generated by drop casting in KBr discs after evaporating the solvent) using a Perkin-Elmer FTIR spectrophotometer (model spectrum RX I), within a range of 400–4400 cm^{-1} at a resolution of 4 cm^{-1}. FTIR of clays powder was done by preparing KBr plates by taking 1:4 clay and KBr. An average of 16 scans was reported for each sample.

Mechanical testing

The tensile properties of the CPE composites were measured by a Universal Testing Machine (Hounsfield 10KS) at a crosshead speed of 500 mm/min at room temperature according to ASTM D 412-98. Tensile strength, tensile modulus, and elongation at break were recorded. The average values of three tests are reported for each sample.

Dynamic mechanical thermal analysis

Dynamic mechanical thermal analysis of the rubber composites with Cloisite 30B and Cloisite 15A were carried out by using a Q800 dynamic mechanical thermal analyzer of TA Instruments (USA). The sample specimens (30 × 10 × 1.5 mm^3) were analyzed in tensile mode at a constant frequency of 1 Hz, at 0.1% strain in the temperature range of −80 to 80 °C at a heating rate of 3°C/min. Storage modulus (E'), loss modulus (E''), and loss tangent (tan δ) were measured as a function of temperature for all the samples under identical conditions.

Differential scanning calorimetric analysis

Differential scanning calorimetric (DSC) studies were carried out in TA Instruments (model Q 100V 8.1) at a heating rate of 20 °C/min under nitrogen atmosphere in the temperature range of −70 to 200 °C. The second heating scans of all the samples were reported to nullify the thermal history. The data were analyzed by a TA Universal analysis software on TA computer attached to the machine. The transitions were detected from the occurrence of discontinuity in the curves. The average of three tests is reported here.

Thermogravimetric analysis

Thermogravimetric analysis (TGA) was carried out in TA Instruments (model Q 50), at a heating rate of 20 °C/min under air atmosphere up to 800 °C. A small amount of material (around 5 mg) was used for the TGA study. The data were analyzed by TA Universal analysis software on a TA computer attached to the machine. The average of three tests is reported here. The error of the measurements was ±1 °C.

Results and discussion

Morphology study of CPE–clay nanocomposites

Figure 1a shows WAXS patterns of CPE/Na^+MMT nanocomposites. The as-received Na^+MMT shows a strong peak at $2\theta = 7.2°$, which corresponds to a basal spacing $d_{001} = 1.22$ nm. The interlayer distance in the clays alone and in the clay nanocomposites was determined by the first diffraction peak of X-ray patterns by the Bragg equation. In presence of CPE, the peak moves to lower angles, reflecting significant intercalation; d_{001} at 5 wt% loading of Na^+MMT is 3.48 nm, whereas at 10 and 20 wt% loading of the clay the basal spacing (d_{001}) values are 2.46 and 1.84 nm, respectively.

Figure 1b shows WAXS spectra for CPE/Na^+MMT (5 wt%), CPE/Cloisite® 30B (5 wt%) and CPE/Cloisite® 15A (5 wt%) composites. The organically modified MMT again undergoes significant expansion at very low clay loading of 5 wt%. The XRD confirms the separation of clay particles in CPE/30B compounds. The clay peak of CPE/Cloisite® 30B is broadened and shifted to a lower angle of $2\theta = 1.84°$, which is equivalent to d spacing of 4.80 nm in comparison with the original d spacing of 1.90 nm of Cloisite® 30B clay. The substantial reduction in intensity and the shift at lower 2θ angles of the 001 peak of the Cloisite® 30B indicates that the interlayer spacing of the organophilic clay increases due to the intercalation of the polymer chains [27]. These results are similar to the work on other elastomeric systems [15, 26]. No characteristic peak of the clay is observed in the XRD patterns of the composites of Cloisite15A in comparison with the gallery distance of 3.40 nm for the Cloisite® 15A. This indicates that the clay layers are not at all stacked in the composites, but homogeneously dispersed in the polymer

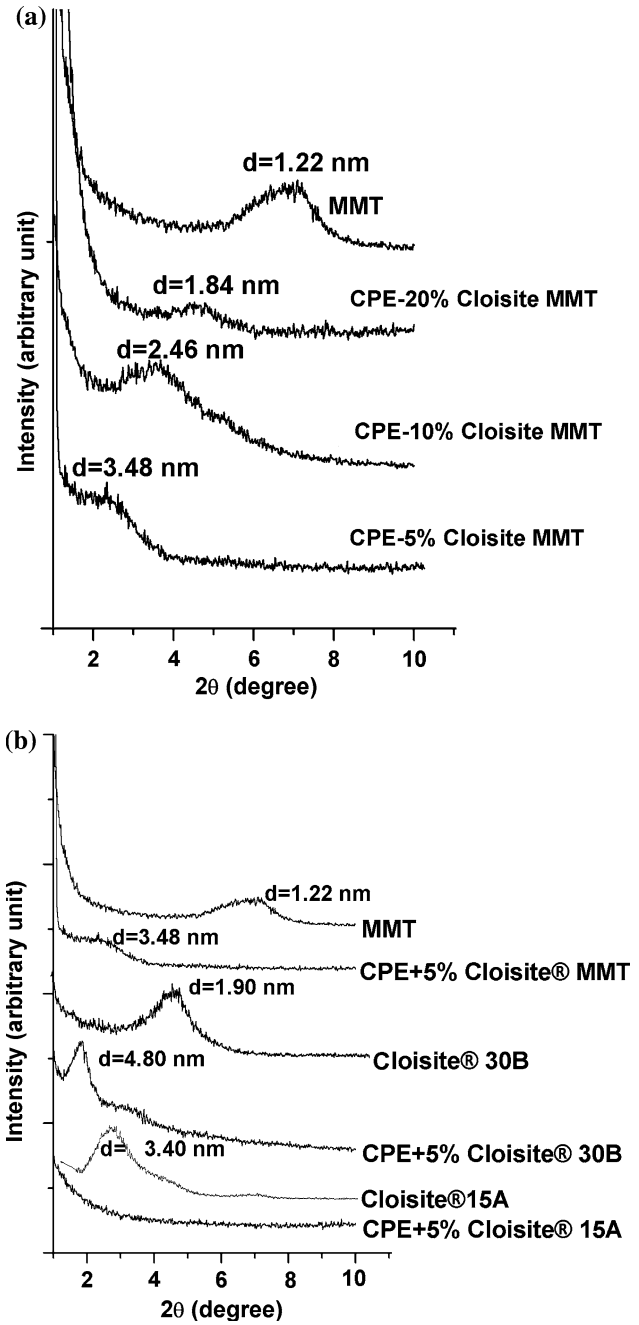

Fig. 1 **a** XRD of CPE/MMT nanocomposites, **b** XRD of CPE/clay nanocomposites

matrix (exfoliated nanocomposites) due to the better compatibility of the Cloisite®15A clay with CPE and larger initial gallery distance. As seen in Table 1, Cloisite® 15A surface is modified with onium ion at an excess amount, whereas the Cloisite® 30B surface is less saturated with intercalant. As a result of the difference in intercalant chemistry and level of modification, the clay galleries are opened to different extents, as indicated by the gallery distances.

Figure 2 shows representative TEM micrographs of various nanocomposites. At 20 wt% loading of Na^+MMT, the clay layers are almost stacked together (Fig. 2a). But at 5 and 10 wt% loading, the clay layers appear to be intercalated (Fig. 2b, c). In Fig. 3, TEM micrographs of CPE nanocomposites with 5 wt% of 15A and 30B separately are illustrated. With 5 wt% loading of 30B, highly intercalated morphology (Fig. 3a) is found. Figure 3b illustrates the intercalated nanocomposite of 30B at high magnification. The apparently visible crosshatched network is a perpendicular view of the three-dimensional clay layers crossing each other, which are possibly separated by the CPE matrix. For 5% loading of 15A, a fully exfoliated structure (Fig. 3c) is observed, which supports XRD data. Interestingly, it has been found that preferred quaternary ammonium compounds for the preparation of the nanocomposites are those apparently wherein there are two alkyl groups each having about 12 to about 22 carbon atoms and 2 methyl groups. Hence, between Cloisite® 30B and Cloisite® 15A, the preferred quaternary ammonium compound is Cloisite® 15A, which is dimethyl di (hydrogenated tallow) ammonium chloride. These characteristics are supported further by the FTIR results (discussed later), showing the interaction between the CPE matrix and the clay surfactants of Cloisite® 30B and Cloisite® 15A and hydroxyl groups of clays. Effect of the morphology is reflected in the mechanical and thermal properties of the nanocomposites.

Mechanical properties

Representative stress–strain curves for the nanocomposites are depicted in Fig. 4. Incorporation of layered silicates in rubber leads to an increase in tensile strength and modulus, as shown in Fig. 4. In this plot, the sample, in which surface-modified clays are used, displays a marginal reduction in strain-to-failure. However, it is interesting to note that the tensile strength of the 5% Cloisite® 15A loaded CPE appears to be superior to those of 5% Cloisite® 30B and 5% Na^+MMT loaded CPE. An increase in modulus in presence of clays, particularly modified clays, is observed (Table 3). Maximum modulus is found at 5% Cloisite® 15A content, indicating that the modulus increases when clay layers are exfoliated in the CPE matrix, and the surfactant of the modified clay makes a better interaction with the rubber matrix.

The reinforcing effect of the clays is more noticeable at 200 and 300% strains for both the composite systems with 5% modified clays. In Fig. 4, the modulus of CPE-D at 200 and 300% strains are higher than those of CPE-B1 and CPE-C (Table 3). It is found that the average 200% modulus of the modified clay nanocomposites, particularly the 5% Cloisite® 15A-modified CPE, increases about 4.5 times

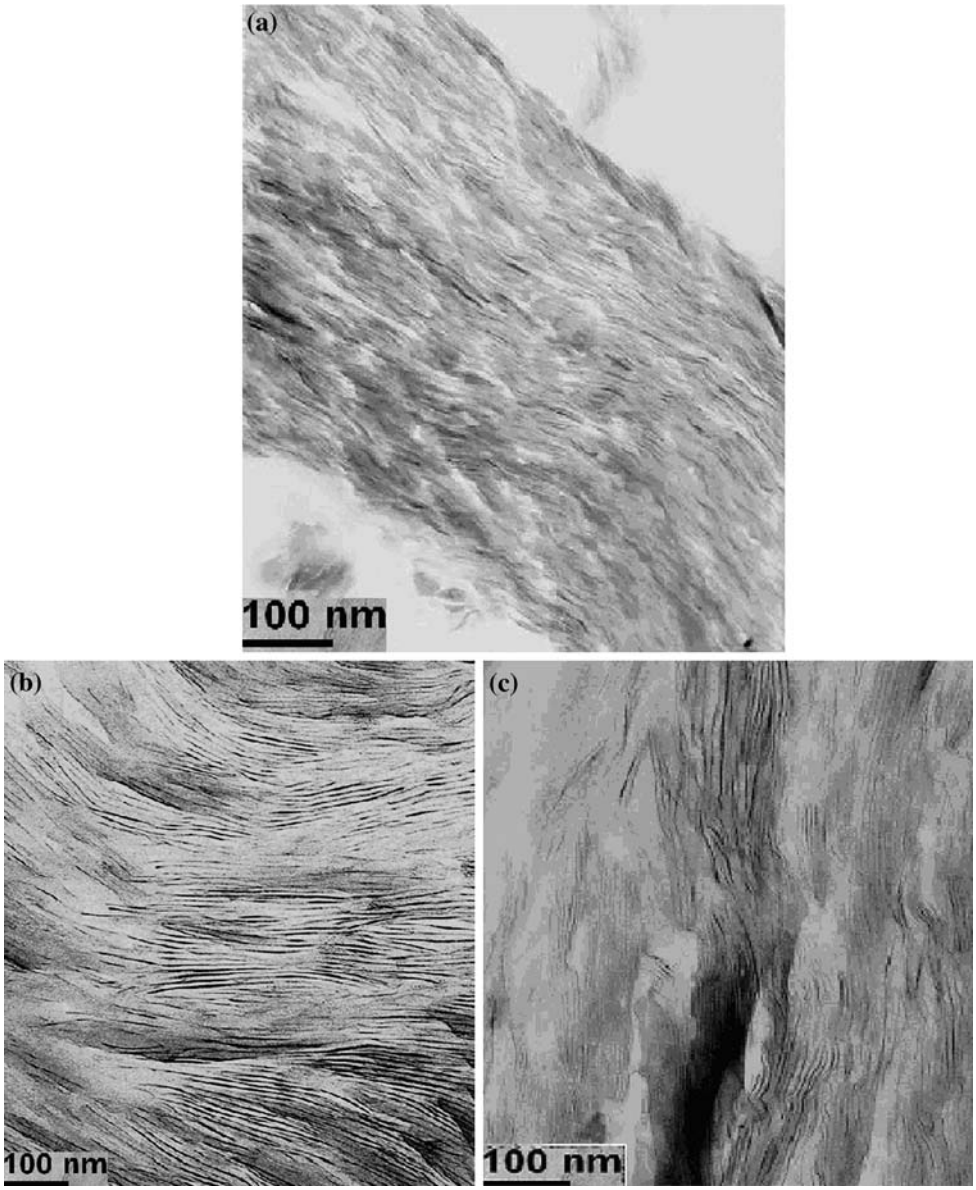

Fig. 2 TEM photographs of CPE nanocomposites with **a** 20 wt%, **b** 10 wt%, and **c** 5 wt% Na^{+}MMT loading

over the neat rubber and almost three times over Na^{+}MMT-modified CPE (Table 3). At 300% strain, the average modulus of CPE-D at 25 °C is 4.5 times higher than that of CPE-A, whereas the CPE-C exhibits a value almost three times higher compared to that of CPE-A. Data in Table 3 show lower values of both tensile strength and modulus in CPE-C as compared to those of CPE-D.

It is worth noting that the high modulus of CPE-C and CPE-D nanocomposites is due to the reinforcement mechanism in the CPE rubber by the modified clays, which appears to be more obvious at higher strain levels. This is because as the strains become larger, the presence of nanoparticles could restrict the number of possible configurations, thus leading to a stiffer rubber [28, 29]. The exfoliation of the layers of that of 15A clay due to better interaction of the clay surfactant with the rubber matrix also gives rise to the increase in modulus. The increased stiffness may be caused by the formation of the immobilized rubber phases due to the exfoliation of the clay platelets.

DMTA analysis

The mechanical behavior of the materials over a range of temperatures was characterized by DMTA, and the resulting curves for the neat CPE rubber compound and the nanocomposites CPE-B, CPE-C, and CPE-D are shown in Fig. 5. In general, the three materials show a similar trend, including the glass transition, as clearly reflected in the tan δ curve. However, at temperatures below 10 °C, the nanocomposites have a higher storage modulus, and the modulus of CPE-D is slightly higher than that of CPE-C,

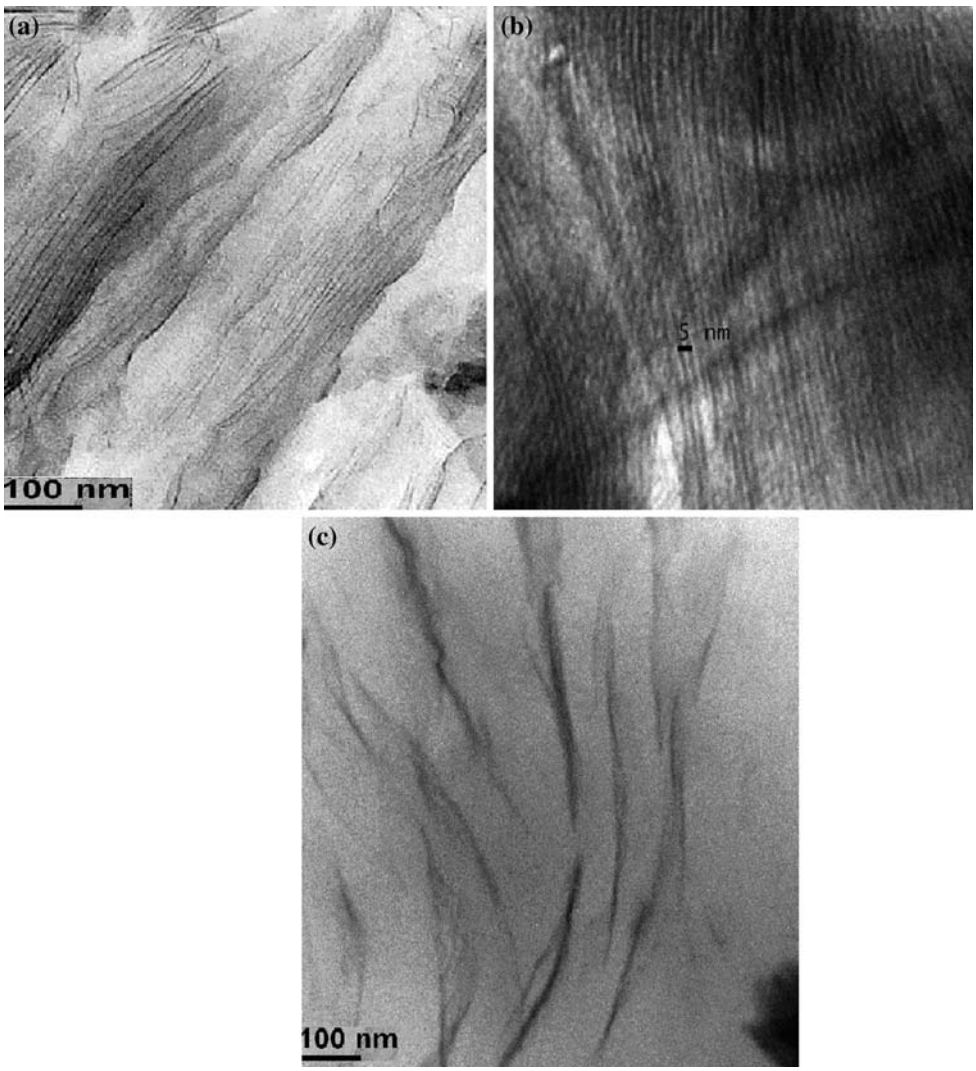

Fig. 3 TEM photographs of CPE nanocomposites of **a** 5 wt% Cloisite® 30B at low magnification, **b** 5 wt Cloisite® 30B at high magnification, and **c** 5 wt% Cloisite® 15A

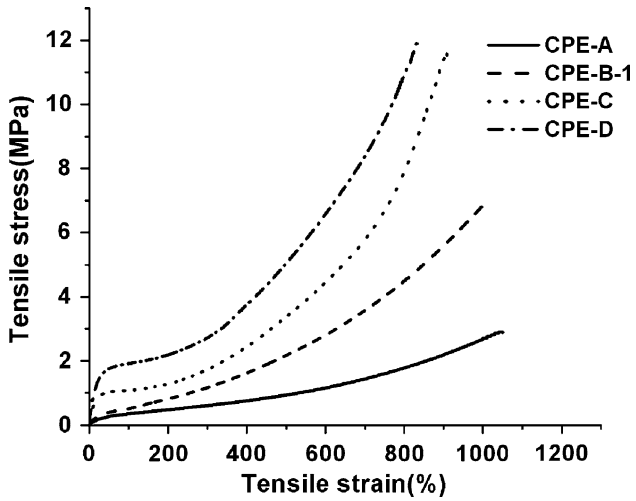

Fig. 4 Tensile stress–strain plot for CPE–clay nanocomposites

Table 3 Mechanical properties of CPE–clay nanocomposites

Compound designation	CPE-A	CPE-B-1	CPE-C	CPE-D
Tensile strength (MPa)	2.88	6.91	11.4	11.9
Elongation at break (%)	1050	1000	910	830
Modulus at 100% elongation (MPa)	0.35	0.51	1.08	1.92
Modulus at 200% elongation (MPa)	0.48	0.82	1.28	2.19
Modulus at 300% elongation (MPa)	0.61	1.17	1.73	2.72

which is in line with the room temperature tensile moduli of Fig. 4.

Tan δ and elastic modulus (E') obtained from DMTA are shown in Table 4. As shown in Fig. 5, all the CPE composites have a relaxation around 3–8 °C, which is

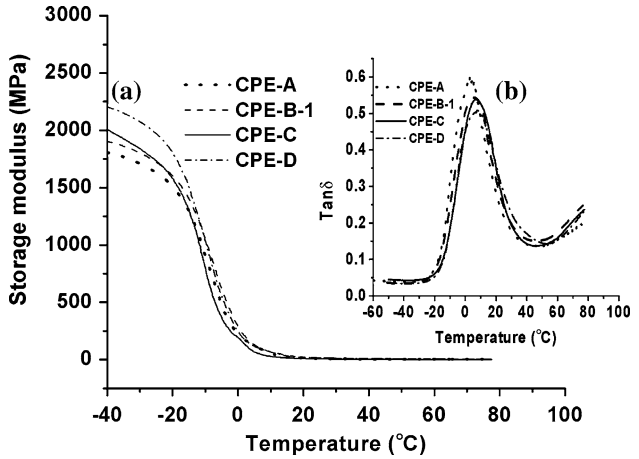

Fig. 5 Plot of **a** storage modulus and **b** tan δ versus temperature of CPE–clay nanocomposites

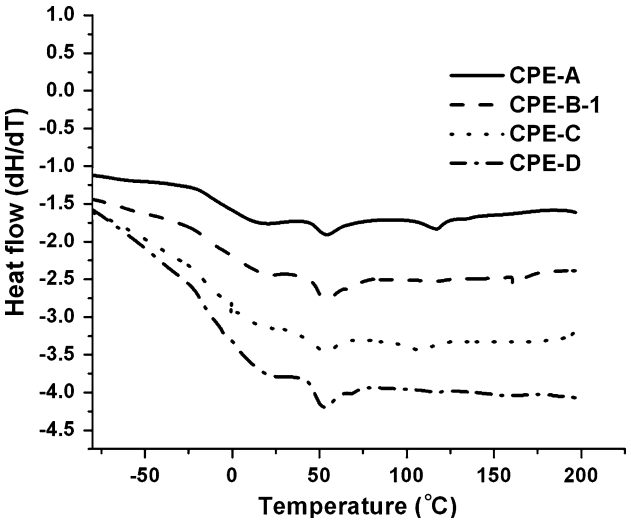

Fig. 6 DSC plot of CPE–clay nanocomposites

Table 4 Dynamic mechanical of CPE–clay nanocomposites

Compound designation	Tan δ at T_g	Storage modulus at −40 °C (MPa)	T_g (°C)
CPE-A	0.60	1812	3
CPE-B-1	0.54	1904	5
CPE-C	0.53	2011	6
CPE-D	0.50	2202	8

related to the glass-transition temperature (T_g). A gradual decrease in tan δ value is observed from CPE-A to CPE-D, which indicates that the damping nature of the polymer decreases with increase in interaction between the polymer and the clay. CPE-A presents a T_g at 3 °C, which is shifted to higher temperature in the case of CPE–clay nanocomposites (5 °C for CPE-B and 6 °C for CPE-C and 8 °C for CPE-D). The presence of clay platelets increases the interaction and thereby restrains the mobility of the rubber chains, as expected.

It is clear that the storage modulus at −40 °C temperature is increased by 5% for CPE-B, 10% for CPE-C, and 21% for CPE-D nanocomposites. The effect of the modified clays is very significant in the storage modulus of the CPE nanocomposites mainly in the transition region and the rubbery plateau. The storage modulus values of the clay composites suggest an effective dispersion of the nano layers of clays in the elastomeric matrix, which is more prominent in the case of Cloisite® 15A, which exfoliates completely in the CPE matrix due to its better interaction with the CPE.

Thermal properties

Flame-retardant composites were analyzed by DSC and TGA. The DSC curves of CPE-A, CPE-B-1, CPE-C, and CPE-D are shown in Fig. 6. The results clearly reveal the heat flow difference between CPE-A and CPE-B is much higher than that of the CPE-A and CPE-C or CPE-A and CPE-D. Since dt/dT is constant and the sample mass is the same, the specific heat of CPE-C and CPE-D is greater than that of CPE-B-1.

This phenomenon can be explained as the clays that have better interaction with the matrix can absorb more heat. Also, the increase in heat flow difference of the nanocomposites becomes more substantial with increased temperatures, which means at high temperature the nanocomposites can better resist heat than CPE-A. On the other hand, the increase in heat flow difference indicates that the nanocomposites can absorb more heat during the heating and would improve the thermal stability of CPE–clay nanocomposites.

The substantial improvement in the thermal characteristics of the nanocomposite over the CPE-A is again established by TGA which shows how the increasing specific heat translates into improved degradation characteristics. Figure 7 represents TGA traces and their derivatives for CPE-A, CPE-B, CPE-C, and CPE-D. All these samples undergo two degradation steps, as shown in Fig. 7. The onset temperature (T_i) and the 30% weight-loss temperature (T_{30}) residue at 750 °C and rate of degradation are listed in Table 5. This table reveals that CPE–clay nanocomposites show a distinct increase in T_i. The major difference between the unmodified polymer and the nanocomposites is the weight loss after 550 °C. The residue of the sample is increased. Among them, the sample CPE-D with 5 wt% 15A has the highest residue at 750 °C. As shown in Fig. 7a, degradation begins at 273 °C in the case of Cloisite® 30B and at 287 °C for Cloisite 15A nanocomposites. Lower thermal stability of CPE-C in

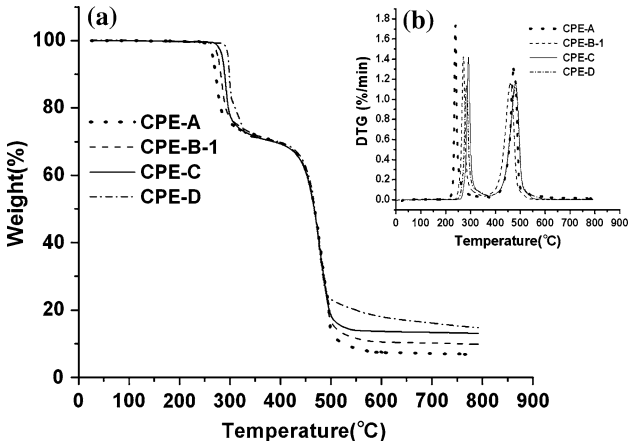

Fig. 7 Plot of **a** TGA and **b** DTG of CPE–clay nanocomposites

Table 5 Thermal properties of CPE–clay nanocomposites

Sample	T_i (°C)	$T_{30\%}$ (°C)	Residue (%) at 750 °C	Rate of degradation (%/min)
CPE-A	250	418	7	1.72
CPE-B-1	264	421	10	1.42
CPE-C	273	427	13	1.41
CPE-D	287	431	15	1.13

comparison to CPE-D is possibly due to the degradation of the intercalants and better interaction between the clay and the polymer in the later case. It is well known that the unsaturated bonds in the tallow moiety of the intercalant in this clay are sensitive to degradation at temperatures above 180 °C. The analogous weight-loss curves also reflect the thermal stability by using CPE/15A nanocomposites mainly due to the physical process in condensed phase.

Figure 7b shows the derivative thermograms (DTG), which gives rate of degradation in the heating process. It can be seen that the weight-loss rates obtained from the samples using CPE/clay nanocomposites (samples CPE-B to CPE-D) are much smaller than that of using neat CPE rubber compound as polymer matrix (sample CPE-A). Among them, the sample CPE-D with 5 wt% Cloisite® 15A has the smallest weight-loss rate.

These TGA results and DSC plots testify that nanodispersed lamellae of clays (exfoliation or intercalation) in CPE rubber matrix have the main flame-retardant effect. An ablative reassembling of the silicate layers may occur on the surface of a burning nanocomposite, creating a physical protective barrier on the surface of the material [30, 31] and can limit the oxygen diffusion to the substrate or give a less-disturbing low volatilization rate. Accordingly, the rate of thermal decomposition is decreased from CPE-A (1.72%/min) to CPE-D (1.13%/min) with increase in interaction between clay layers and CPE matrix. Above the temperature of 30% degradation, residues are increased.

FTIR spectroscopic studies

Figure 8 shows the full-scale FTIR spectrum of CPE, Cloiste Na, CPE with 5 phr of Cloiste Na, Cloisite 30B, CPE with 5 phr of Cloisite 30B, Cloisite 15A and CPE with 5 phr of Cloisite 15A. CPE is characterized by characteristic absorption peaks at 2800–3000 cm^{-1} of –CH– and $–CH_2$ stretching frequencies, 1470 cm^{-1} of $–CH/–CH_2$ bending frequency and 700–500 cm^{-1} of C–Cl stretching frequencies. The peaks at 670 and 540 cm^{-1} confirm the C–Cl linkage in the polymer backbone. The clay particles in the nanocomposites exhibit characteristic bands associated with the stretching of structural –OH stretching peak (e.g., from the Al–OH bond) at 3620, 3400–3200 cm^{-1} (bonded –OH and –NH– stretching), Si–O (1018 cm^{-1}), Si–O–Al (525 cm^{-1}), and bending of Si–O–Si at 465 cm^{-1}, as shown in Figs. 8 and 9. To see the effect of hydrogen bonding with –Cl groups, the FTIR spectra have been enlarged in the region 1500–400 cm^{-1}. It is interesting to see that the characteristic peak of C–Cl moves to the lower wavenumber region in CPE with Cloisite 30B and CPE with Cloisite 15A due to the hydrogen bonding with the –OH/–NH– groups of clay. Comparison between CPE and CPE with Cloisite Na in Fig. 9 indicates that the characteristic peak of C–Cl absorptions of CPE remains

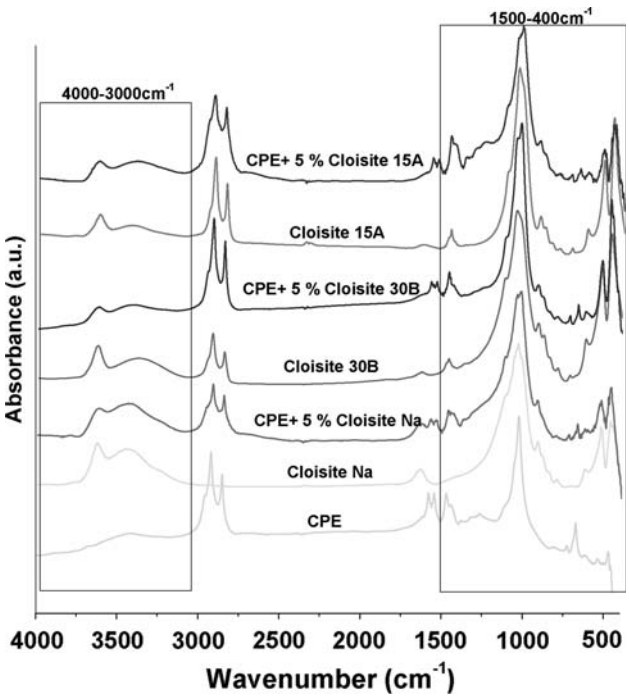

Fig. 8 Full-range FTIR spectra of CPE, different clays, and CPE mixed 5 phr of different clays

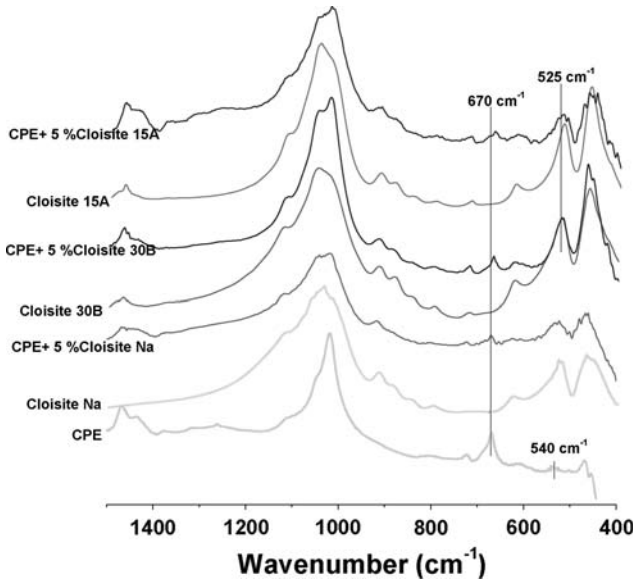

Fig. 9 FTIR spectra of lower wavenumber region of CPE, different clays, and their composites

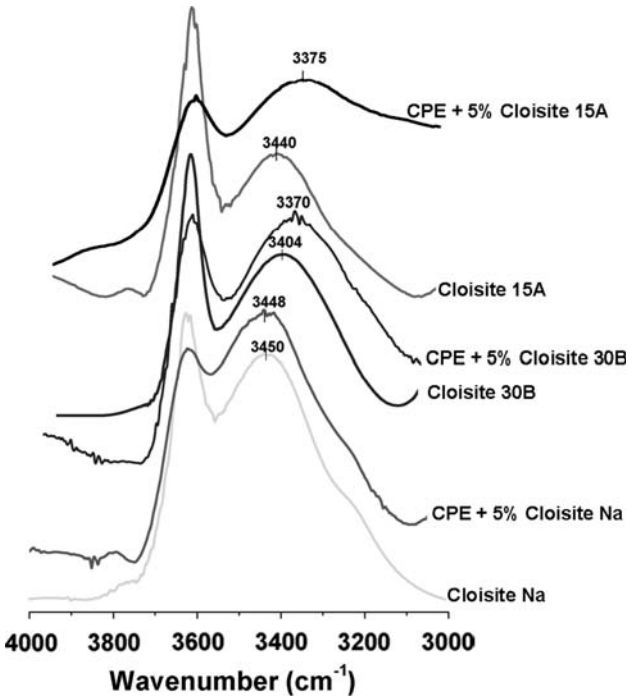

Fig. 10 FTIR spectra (hydroxyl stretching region) of different clays and CPE mixed 5 phr of different clays

unchanged. This observation reveals low interaction between the CPE and the unmodified clay as there is no organic intercalant in the Cloisite Na. The organic intercalant, i.e., ternary ammonium salt (in the case of Cloisite 30B and Cloisite 15A) is responsible for the hydrogen bonding with –Cl groups in the polymer chains. The peak at 540 cm^{-1} of the C–Cl of pristine CPE merged with the peak 525 cm^{-1} of the clay in the nanocomposites. To further prove the H-bonding, enlarged FTIR spectra between 4000 and 3000 cm^{-1} of Cloisite Na, CPE with Cloisite Na, Cloisite 30B, CPE with Cloisite 30B, Cloisite 15A and CPE with Cloisite 15A (Fig. 10) are considered. The stretching frequency of structural –OH at 3620 cm^{-1} remains unchanged in clays and their nanocomposites. The absorption peak of –OH/–NH– groups in the region 3500–3200 cm^{-1} is shifted from their original position for the modified clay nanocomposites. For CPE with Cloisite 30B, the peak is shifted to 3370 cm^{-1} from 3404 cm^{-1}. Similarly, in CPE with Cloisite 15A peak also, there is a shift from 3440 to 3375 cm^{-1}. But there is little change in the peak position of Cloisite Na and CPE with Cloisite Na, due to the low interaction between matrix and clay. The alkyl ammonium groups in the modified clay facilitate the formation of H-bonding in the nanocomposites, leading to more interaction with the polymer matrix. Chrissopoulou et al. [28] show the H-bonding type interaction with maleated PP and modified clay in PP clay nanocomposites. The H-bonding is responsible for pseudo crosslinking between the CPE matrix and the modified clay. The adherence of the polymers to the nanoclay facilitates the reversibility of the crosslinkages. Vo and Giannelis [29] also show the interaction between the modified clay and the poly(vinylidene fluoride) in poly(vinylidene fluoride)/nylon-6/clay nanocomposites by DSC study.

Conclusions

The role of organically modified clays in the nanocomposites based on CPE matrix has been thoroughly investigated in this article. The modified MMT clays (Cloisite® 30B and Cloisite® 15A) were well dispersed in CPE. The polarity of chlorinated polymer chains and organophilicity of the organically treated MMT clay allowed formation of excellent polymer nanocomposites. CPE–clay nanocomposites showed an improvement in Young's modulus, storage modulus, and thermal stability in presence of these clays. Cloisite® 15A exhibited outstanding results in this respect. The nanocomposites with 5 wt% Cloisite® 15A had the best thermal and mechanical properties. Its strength was 11.9 MPa and elongation at break was 835%. Its modulus at 200% strain was increased by 4.5 times over the neat CPE rubber compound and the storage modulus of CPE-D at −40 °C was increased by 21%. The TGA curves also reflected the thermal stability of the nanocomposites mainly due to the physical processes in the condensed phase. IR spectroscopic data suggested the existence of interfacial reaction between the clay layers intercalants and the CPE rubber.

References

1. Usuki A, Kawasumi M, Okada A (1993) J Mater Res 8:1174
2. Usuki A, Kojima Y, Kawasumi M, Okada A (1993) J Mater Res 8:1179
3. Fornes TD, Yoon PJ, Keskkula H, Paul DR (2001) Polymer 42:9929
4. Hasegawa N, Kawasumi M, Kato M, Usiki A, Okada A (1998) J Appl Polym Sci 67:8792
5. Aranda P, Ruiz-Hitzhy E (1999) Appl Clay Sci 15:119
6. Sandi G, Carrado KA, Joachin H, Lu W, Prakash J (2003) J Power Sources 119:492
7. Yano K, Usuki A, Okada A, Kurauchi T, Kamigaito O (1993) J Polym Sci A Polym Chem 31:2493
8. Donnet JB (2003) Compos Sci Technol 63:1085
9. Zhang LQ, Wu YP, Wang YQ (2000) China Synth Rubber Ind 23:71
10. Hamed GR (2000) Rubber Chem Technol 73:524
11. Zhang L, Wang Y, Wang Y, Sui Y, Yu D (2000) J Appl Polym Sci 78:1873
12. Wang Y, Zhang L, Tang C, Yu D (2000) J Appl Polym Sci 78:1879
13. Wu Y-P, Zhang L-Q, Wang Y-Q, Liang Y, Yu D-S (2001) J Appl Polym Sci 82:2842
14. Maiti M, Bhowmick AK (2006) Polymer 47(17):6156
15. Maiti M, Bhowmick AK (2007) J App Polym Sci 105(2):435
16. Maji PK, Guchhait PK, Bhowmick AK (2009) ACS Appl Mater Interface 1:289
17. Usuki A, Tukigase A, Kato M (2002) Polymer 43:2185
18. Acharya H, Srivastava SK, Bhowmick AK (2007) Compos Sci Technol 67(13):2807
19. Arroyo M, Lopen-Manchado MA, Herrero B (2003) Polymer 44:2447
20. Varghese S, Karger-Kocsis J (2003) Polymer 44:4921
21. Ganter M, Gronski W, Reichert P, Muelhaupt R (2001) Rubber Chem Technol 74:221
22. Ganguly A, De Sarkar M, Bhowmick AK (2006) J Polym Sci B Polym Phys 45(1):52
23. Kim Y, White JL (2003) J Appl Polym Sci 90:1581
24. Datta H, Singha NK, Bhowmick AK (2008) Macromolecules 41:50
25. Patel S, Bandyopadhyay A, Vijayabaskar V, Bhowmick AK (2005) Polymer 46:2005
26. Sadhu S, Bhowmick AK (2004) J Polym Sci B Polym Phys 42:1573
27. Giannelis EP, Krishnamoorti R, Manias E (1999) Adv Polym Sci 118:108
28. Chrissopoulou K, Altintzi I, Andrianaki I, Shemesh R, Retsos H, Giannelis EP, Anastasiadis SH (2008) J Polym Sci B Polym Phys 46:2683
29. Vo LT, Giannelis EP (2007) Macromolecules 40:8271
30. Zanetti M, Kashiwagi T, Falqui L, Camino G (2002) Chem Mater 14:881
31. Wang SF, Hu Y, Lin ZH, Gui Z, Wang ZZ, Chen ZY, Fan WCH (2003) Polym Int 52:1045